AGU100 ADVANCING EARTH AND SPACE SCIENCE

Geophysical Research Letters

RESEARCH LETTER
10.1002/2018GL077382

Key Points:
- For the first time we combine process-based models of the CH_4 cycle as priors, with ice core observations in a Bayesian framework
- For the glacial we infer unchanged or increased geological sources, but a halved wetland flux, which is not captured by process modeling
- This suggests missing processes in methane models, with potentially important consequences for confidence in future methane projections

Supporting Information:
- Supporting Information S1

Correspondence to:
P. O. Hopcroft,
p.hopcroft@bham.ac.uk

Citation:
Hopcroft, P. O., Valdes, P. J., & Kaplan, J. O. (2018). Bayesian analysis of the glacial-interglacial methane increase constrained by stable isotopes and Earth System modeling. *Geophysical Research Letters*, *45*, 3653–3663. https://doi.org/10.1002/2018GL077382

Received 6 FEB 2018
Accepted 5 MAR 2018
Accepted article online 12 MAR 2018
Published online 22 APR 2018

Bayesian Analysis of the Glacial-Interglacial Methane Increase Constrained by Stable Isotopes and Earth System Modeling

Peter O. Hopcroft[1,2,3], **Paul J. Valdes**[1,2], **and Jed O. Kaplan**[4,5]

[1]Bristol Research Initiative for the Dynamic Global Environment, School of Geographical Sciences, University of Bristol, Bristol, UK, [2]Cabot Institute, University of Bristol, Bristol, UK, [3]Now at the School of Geography, Earth and Environmental Sciences, University of Birmingham, Edgbaston, UK, [4]Max Planck Institute for the Science of Human History, Jena, Germany, [5]ARVE Research SARL, Pully, Switzerland

Abstract The observed rise in atmospheric methane (CH_4) from 375 ppbv during the Last Glacial Maximum (LGM: 21,000 years ago) to 680 ppbv during the late preindustrial era is not well understood. Atmospheric chemistry considerations implicate an increase in CH_4 sources, but process-based estimates fail to reproduce the required amplitude. CH_4 stable isotopes provide complementary information that can help constrain the underlying causes of the increase. We combine Earth System model simulations of the late preindustrial and LGM CH_4 cycles, including process-based estimates of the isotopic discrimination of vegetation, in a box model of atmospheric CH_4 and its isotopes. Using a Bayesian approach, we show how model-based constraints and ice core observations may be combined in a consistent probabilistic framework. The resultant posterior distributions point to a strong reduction in wetland and other biogenic CH_4 emissions during the LGM, with a modest increase in the geological source, or potentially natural or anthropogenic fires, accounting for the observed enrichment of $\delta^{13}CH_4$.

Plain Language Summary Methane is the next most important greenhouse gas in the atmosphere after carbon dioxide. Since industrialization, methane has risen from around 680 ppbv (parts per billion volume) to 1,800 ppbv today. Before industrialization, methane levels were dominated by natural processes. The largest recent changes occurred during ice age to interglacial transitions. Measurements on gas bubbles preserved in ice cores show that methane rose with global temperatures, from around 375 ppbv during the ice age, to 680 ppbv prior to the Industrial Revolution. Explaining this amplitude remains a challenge, because there are no measurements of past sources or sinks of methane. Stable isotopes of methane provide additional information, because different sources and sinks impart unique signatures to the methane measured in ice cores. We use these measurements with a computer model of the global methane cycle. We then employ a statistical approach to learn how sources changed, taking account of uncertainties. We find that a near doubling of the wetland methane source is required. This is much greater than the change simulated in this and other methane models. This potentially indicates that methane models are undersensitive, with implications for understanding how the methane cycle will evolve in the near future.

1. Introduction

Atmospheric methane (CH_4) is an important greenhouse gas. Its concentration has risen sharply over the past two centuries, reaching 1,799 ppbv by Common Era (CE) 2010 (Kirschke et al., 2013). This is estimated to have contributed around 25% of the anthropogenic greenhouse gas effect since CE 1750 (Myhre et al., 2013). CH_4 is also reactive with a lifetime of about 9 years (Prather et al., 2012), and so its abundance indirectly affects the concentrations of other trace gases such as nitrous oxide and ozone.

Observed variations in the growth rate over the past decades are not well understood (e.g., Bousquet et al., 2011; Kirschke et al., 2013). Different studies have implicated changes in biogenic emissions (e.g., Nisbet et al., 2016; Schaefer et al., 2016), lifetime (Rigby et al., 2017) or biomass burning emissions (Worden et al., 2018) in the recent growth rate. Prior to the observational era, changes in atmospheric methane can be accurately reconstructed from gas bubbles recovered in ice cores. During the late Quaternary, CH_4 mixing ratios are correlated with climate (e.g., Loulergue et al., 2008). Explaining the magnitude of these variations remains a challenge

(Hopcroft et al., 2017; Levine, Wolff, Jones, Sime, Valdes, et al., 2011; Murray et al., 2014), reflecting incomplete understanding of the source and sink processes.

The increase in atmospheric CH_4 concentration from the LGM to the beginning of the Industrial Revolution (hereafter the late preindustrial) is among the largest such changes, with an increase from 375 ppbv to 680 ppbv (Loulergue et al., 2008; Mitchell et al., 2013; WAIS Divide Project Members, 2015). This concentration increase is likely the result of a near doubling of the source of methane (Levine, Wolff, Jones, Sime, Valdes, et al., 2011; Murray et al., 2014). Considerable debate remains over how this occurred (Kaplan et al., 2006; Levine, Wolff, Jones, Sime, Valdes, et al., 2011; Murray et al., 2014; Valdes et al., 2005), because of uncertainties in the response of methane sources and sinks to climate, and in terms of the relative importance of different sources in the late preindustrial era (Hopcroft et al., 2017).

Concurrent changes in the stable isotopes of methane can provide additional constraints, because different sources and sinks of methane have distinct isotopic signatures and fractionation rates (e.g., Bock et al., 2017). Between the LGM and preindustrial, $\delta^{13}CH_4$ became depleted from -43 ± 0.3‰ to -48 ± 0.3‰, with a similar depletion of deuterium of CH_4 (δDCH_4) from -79 ± 4‰ to -98 ± 3‰ (Fischer et al., 2008; Möller et al., 2013; Sowers, 2006, 2010).

Fischer et al. (2008) used a box model of atmospheric CH_4 and CH_4 isotopes and adjusted the relative contributions of sources and sinks to explain the observed glacial-interglacial changes. They inferred an increase in wildfire CH_4 emissions (+18%) at the LGM and a reduction in wetland emissions (−41%) and CH_4 lifetime (−32%). The latter is in conflict with most model-based estimates.

More recently, Möller et al. (2013) extended ice core records to 160,000 years Before Present and found that the $\delta^{13}CH_4$ is positively correlated with the atmospheric concentration of CO_2 and not CH_4. This suggests that the observed variations of $\delta^{13}CH_4$ likely arise through the effect of CO_2 and climatic changes on the isotopic fractionation rates of CH_4 sources or sinks (Whiticar & Schaefer, 2007), rather than only by changes in the relative importance of the different source types, as previously assumed (Fischer et al., 2008). Möller et al. (2013) suggest that shifts in the isotopic signature of tropical wetland CH_4 are the main contributor.

Here we use process-based Earth System model simulations of the late preindustrial and LGM methane cycles (Hopcroft et al., 2017, H17 hereafter), to better understand the change in CH_4. We calculate the implied isotopic composition of methane, including the environmentally driven change in the isotopic discrimination of vegetation and hence the isotopic signature of wetland and biomass burning emissions. We combine these results in a Bayesian framework, which allows us to incorporate uncertainty estimates and include prior information.

2. Incorporating Process-Based Estimates of Changes in Methane Sources and Lifetime Into a Model of Atmospheric Methane Stable Isotopes

We use the CH_4 sources as incorporated in the Earth System model simulations of the late preindustrial and LGM with HadGEM2-ES (Collins et al., 2011; HadGEM2 Development Team, 2011, and see supporting information), configured with glacial boundary conditions as described previously (Hopcroft & Valdes, 2015; Singarayer & Valdes, 2010; H17). HadGEM2-ES is a widely used, coupled Earth System model (e.g., Booth et al., 2012; Caesar et al., 2013; Hopcroft & Valdes, 2015; Jones et al., 2011; Kandlbauer et al., 2013). It includes wetlands (Gedney et al., 2004; Marthews et al., 2015) and tropospheric chemistry (O'Connor et al., 2014). Separate models of peatlands (Wania et al., 2010), biomass burning (Kaplan et al., 2016; Pfeiffer et al., 2013), oceans, and termites (Kaplan et al., 2003; Sanderson, 1996) were also used, see the supporting information.

Using the standard wetland scheme, the high-latitude emissions are likely underestimated, as shown by a comparison of CH_4 concentrations for the present day (Hayman et al., 2014). Including the peatland flux leads to a stronger high-latitude source, as well as a larger reduction in total wetland/peatland emissions at the LGM of 42% versus 30% without.

H17 presented three alternative scenarios of LGM fire emissions: standard-fire (simulated with a process-based dynamic vegetation model), standard+LGM humans, which additionally incorporates an empirically based estimate of hunter-gatherer fire activities during the LGM (Kaplan et al., 2016), and low fire, in which LGM fire

Table 1
Preindustrial and Prior and Posterior LGM Methane Sources and Lifetime

		LGM					
		Prior			Posterior		
Sources ($TgCH_4$/year)	Late Preindustrial	Mean	±1 s.d.	ΔLGM (%)	Mean	±1 s.d.	ΔLGM (%)
N extratropical wetland	55	18	4.7	−67	12.0	4.0	−78
Tropical wetland	73	55	14.3	−25	32.0	4.7	−56
S extratropical wetland[a]	11	6.2	—	−44	—	—	
Biomass burning	21	13.5	4.8	−36	16.6	2.0	−21
Termites	20	12	3.1	−40	10.8	3.0	−46
Hydrates	10	10	3.6	0	6.9	2.2	−31
Other geological	10	10	4.6	0	10.5	2.5	5
Oceans[a]	1	0.8	–	−20	–	–	–
Sum	201	126	34	−38	96	18	−52
Total lifetime (yr)	9.7	10.3[b]	0.2	6	10.4[c]	0.1	7

Note. The LGM means and standard deviations are derived from the PDFs shown in the blue curves in Figure 3. The individual prior sink terms are given in Table S4 in the supporting information. Refer to Tables S2 and S3 for isotopic signatures of individual sources and sinks.
[a]Indicates sources not varied as part of the Bayesian algorithm. [b]Calculated using the prior mean LGM fire emissions. [c]Calculated using the posterior mean LGM fire emissions. LGM = Last Glacial Maximum.

emissions are arbitrarily set to 10% of late preindustrial values. Here preindustrial fire emissions are scaled based on ice core evidence and other modeling studies (Ferretti et al., 2005; Thonicke et al., 2005), as described in the supporting information.

We introduce a geological source which comprises mud volcanoes, marine seeps, microseepage, and geothermal methane, which are commonly missing from methane inventories (e.g., Etiope et al., 2008). We reduce the ocean source to 1 $TgCH_4$/year in light of recent observations (Kirschke et al., 2013) and set both the hydrate and geological terms to 10 $TgCH_4$/year (Petrenko et al., 2017; H17). We incorporate OH, soil, and stratospheric sink terms as modeled by H17. We also here include a boundary layer atomic chlorine (Cl) sink, which we set to 3% of the total CH_4 sink (Allan et al., 2007; Platt et al., 2004). The assumed isotopic signature of each source and the fractionation factors for the four methane sinks are listed in Table 1, along with estimated prior and posterior values.

We combine these estimates using a three-box model of atmospheric CH_4 and stable isotopes as described in the supporting information (Lassey et al., 2000; Miller, 2005). The results show a preindustrial CH_4 concentration, $\delta^{13}C$ and δD of 683 ppb, −49.0‰ and −98.4‰ respectively. These are in agreement with ice core

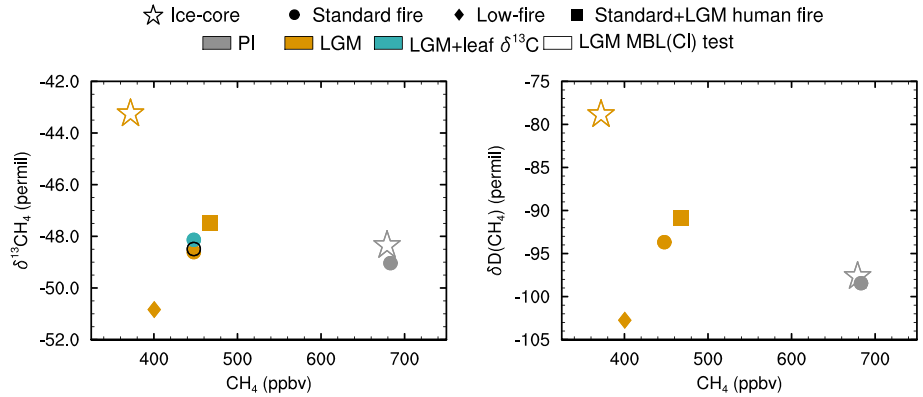

Figure 1. Box model calculations of late preindustrial and Last Glacial Maximum (LGM) CH_4, $\delta^{13}CH_4$, and $\delta^{13}D(CH_4)$. The model is driven with emissions and lifetime derived from HadGEM2-ES climate-chemistry simulations. Ice core data (Fischer et al., 2008; Möller et al., 2013; Sowers, 2006, 2010) are shown by star symbols. Three different model fire estimates for the LGM are shown (low-fire, standard-fire, and standard with LGM human fire).

measurements, as compared in Figure 1. Using LGM fluxes (with standard-fire) results in LGM CH_4, $\delta^{13}C$ and $\delta D(CH_4)$ values of 447 ppbv, −48.6‰, and −93.7‰, respectively, also shown in Figure 1. For both time periods, the box model values are extracted at either the northern or southern box depending on the relevant ice core location, as listed in Table S1. This LGM simulation underestimates both the reduced LGM CH_4 concentration and shift in isotopes. The low-fire scenario in which all fire emissions are set to 10% of the late preindustrial results in a better prediction of the LGM CH_4 change, but at the expense of the $\delta^{13}CH_4$ and $\delta D(CH_4)$, which both shift to more isotopically depleted values. The standard-fire+LGM humans has the opposite effect but is closer to the standard-fire simulation. As a result, to simplify the presentation we only use the standard-fire scenario (filled circles in Figure 1) in the following.

We evaluated the potential influence of changes in the Cl sink following the approach of Levine, Wolff, Jones, and Sime (2011). Using monthly fields from late preindustrial and LGM simulations with HadGEM2-ES (Hopcroft & Valdes, 2015; H17), this results in a small enrichment of $\delta^{13}C$ at the LGM of 0.12‰, shown in Figure 1.

3. Changes in the Isotopic Discrimination by Vegetation and Potential Influence on CH_4 Emissions

During the LGM the $\delta^{13}C$ of atmospheric CO_2 was enriched by 0.1‰ (Schmitt et al., 2012), and thus, this has relatively little impact. More significant are climate-induced variations in the isotopic discrimination by plants (e.g., Kaplan, Prentice, & Buchmann, 2002). Three natural sources of CH_4 (wetlands, biomass burning, and termites) are potentially influenced by the isotopic signature of leaf carbon. For example, C3 and C4 plants exhibit very different leaf carbon isotope ratios. Termites are not observed to show any relationship between emitted $\delta^{13}CH_4$ and the proportion of C3 versus C4 plants (Tyler et al., 1988), so we do not further consider this source term.

Leaf $\delta^{13}C$ is a function of the isotopic discrimination at each stage of gas transfer from the ambient environment to the chloroplasts within the leaf where photosynthesis occurs (Lloyd & Farquhar, 1994). Changes in moisture stress and water use efficiency of a plant will influence the amount of time that stomata are open and hence the overall ratio of intercellular and ambient CO_2. During the LGM, the lower CO_2 significantly reduced plant water use efficiency and is thought to be responsible for around 15% of the total change in $\delta^{13}C$ between the two time periods (Kaplan, Prentice, Knorr, et al., 2002). The lower temperatures and hence potential evaporation and generally drier environment will have competing impacts on the plant available moisture (e.g., Scheff et al., 2017).

We performed late preindustrial and LGM atmosphere-only simulations with HadGEM2-ES similar to those reported previously (Hopcroft & Valdes, 2015; H17) but with new intercellular leaf CO_2 diagnostics (implemented within the dynamic vegetation scheme of Cox (2001), see supporting information, to calculate the isotopic discrimination by vegetation for the two time periods (following Kaplan, Prentice, & Buchmann, 2002; Lloyd & Farquhar, 1994). The resultant leaf to ambient CO_2 ratio and $\delta^{13}C_{leaf}$ anomalies are shown in Figure 2 (weighted by plant functional type fractional coverage). There is a global shift to less negative $\delta^{13}C_{leaf}$ values, from a global average of −26.3‰ to −25.9‰. This is dominated by positive changes in semiarid regions. A reduction in $\delta^{13}C$ during the LGM relative to the late preindustrial in South Africa is in agreement with the model-data comparison of Bragg et al. (2013).

To decompose the drivers of the leaf $\delta^{13}C$ change, we used an updated version of the land surface component of HadGEM2-ES (JULES v4.1: Harper et al., 2016), to quantify the relative influence from changes in climate, atmospheric CO_2, and vegetation, shown in Figure S1. Compared to the globally averaged leaf $\delta^{13}C$ increase of 0.36‰ (which is close to the global average change simulated with HadGEM2), CO_2, climate, and dynamic vegetation separately cause changes of −0.29‰, −0.11‰, and 0.21‰, respectively (and averaged over preindustrial land points only). The CO_2 forced change dominates in the tropics, whereas climate is more significant in midlatitudes. Both of these factors lead to negative excursions for the LGM relative to the preindustrial. The vegetation distribution change has a more widespread and mixed influence, with regions of negative shifts (LGM relative to preindustrial) in leaf $\delta^{13}C$ in southern Africa, western north America, and Eurasia, and positive changes in South East Asia, South America, and Australia.

The isotopic signature of CH_4 emissions was calculated from the weighted sum of the simulated monthly leaf $\delta^{13}C$ values, using either wetland CH_4 emissions or monthly burned area (H17), see Figure 2. We retain

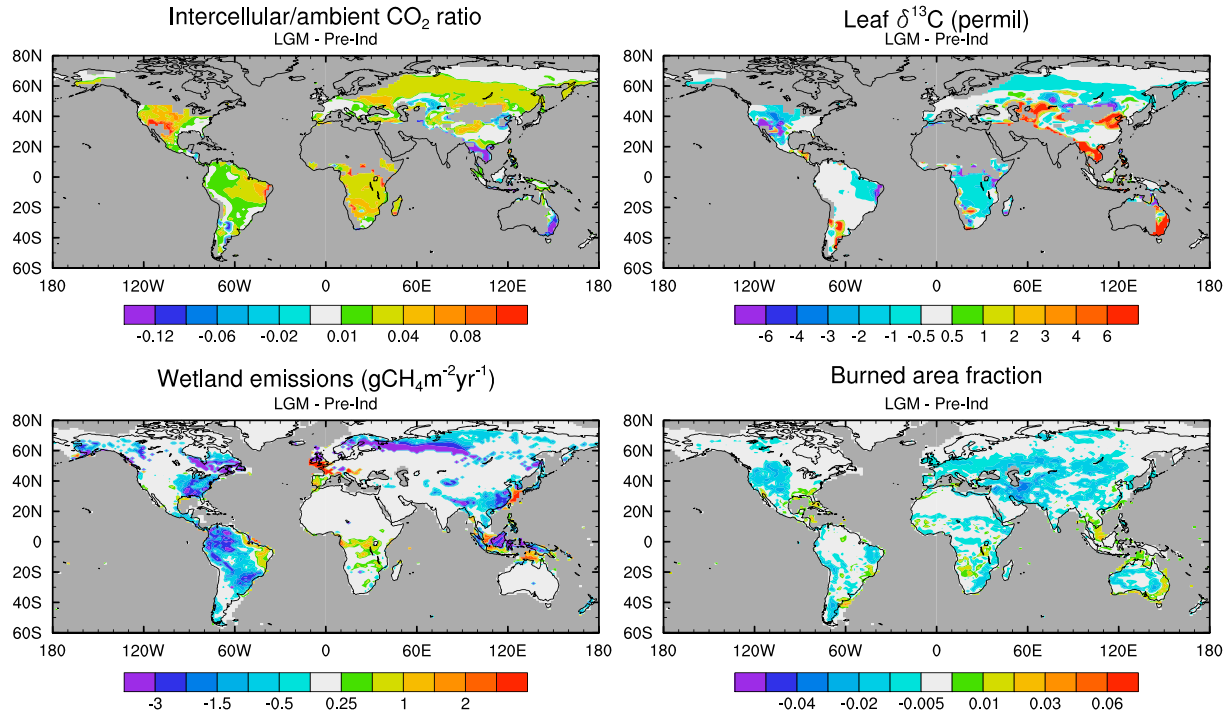

Figure 2. HadGEM2-ES simulated Last Glacial Maximum minus preindustrial anomalies in intercellular/ambient CO_2 ratio, leaf $\delta^{13}C$ (this study) and wetland CH_4 emissions, and burned area fraction (from H17). The CO_2 ratios and $\delta^{13}C$ fields are masked over desert and ice regions. Emissions and burned area anomalies are shown over new land points and where ice sheets change to clarify the role of geographical differences between the two time periods.

the 4‰ difference in $\delta^{13}CH_4$ between tropical and extratropical wetlands and assumed no offset between $\delta^{13}C_{leaf}$ and that of biomass burning (Chanton et al., 2000). We are unable to model this offset for wetland emissions, because, like most global models, JULES does not represent the production, transport, and oxidation of CH_4 isotopes. The $\delta^{13}C$ shift is averaged regionally corresponding with the three-box model.

The global mean wetland source increases by 0.7‰ and the biomass burning source increases by 1.6‰. For wetlands, the change in the distribution of emissions alone, mostly a relocation to the southern extratropics and tropics, causes a shift of 0.9‰. The leaf $^{13}CH_4$ change alone induces a change of 3.3‰. The influence from the assumed offset between the tropical and extratropical wetlands was quantified by setting this difference to zero. It has a strong influence on the result: without this effect the overall signature change is negligible. We find that these separate changes do not combine linearly. For the biomass burning, the change in the global distribution of burning causes a 1.4‰ increase, while the leaf $^{13}CH_4$ change alone causes a 1.3‰ increase.

The isotopic fractionation of CH_4 shows a very small effect from the temperature dependence of fractionation during methanogenesis and methane consumption (following empirical evidence from Tyler et al., 1994) and as described in the supporting information (Blair et al., 1993; Conrad, 2005; Moosavi & Crill, 1998; Schaefer & Whiticar, 2008; Whiticar, 1999). The changes of −0.3‰ and −2‰ for the wetland signature and soil uptake fractionation factor respectively have a negligible impact on the $\delta^{13}CH_4$.

The calculated changes in the isotopic signature of wetland $\delta^{13}C$ averaged in three latitude bands (−0.1, 0.1, and 0.23‰ in the northern, tropical, and southern boxes, respectively) and similarly for biomass burning (2.6, −0.1, and 4.5‰) were included along with the small change in fractionation factors due to the temperature dependence of methanogenesis and uptake in the box model. The zonally averaged values can be summed to give the global total when weighted by changing sources strengths in the three bands, given in Table 1. The results are also shown in Figure 1. The simulated influence of leaf $\delta^{13}C$ on the atmospheric isotopic signature is relatively limited at 0.6‰. This does not capture a substantial fraction of the observed change and implies that changes to both the source mixture and the individual source signatures are required.

4. Inferring Source Changes From Ice Core Observations

To infer the CH_4 sources that are consistent with the ice core observations, we employ a Bayesian framework (e.g., Denison et al., 2002). In this, information from ice cores is combined with the model simulations in a probabilistic formulation which accounts for the estimated uncertainties. We use the model simulations of H17 as prior information and condition the posterior probability density functions (PDFs) for the source strengths using the ice core observations. This approach differs from that of Fischer et al. (2008), because we incorporate prior information rather than sampling unconstrained.

We use a Metropolis-Hastings Markov chain Monte Carlo algorithm (MCMC, see Gilks et al., 1995) to sample the posterior, conditioned on how well the model reproduces the LGM CH_4 concentration and the preindustrial and LGM $\delta^{13}C$ and $\delta D(CH_4)$ values. Assigned observational uncertainties are 2 ppbv, 0.3‰, and 4.0‰ for CH_4, $\delta^{13}CH_4$, and δDCH_4, respectively (Mitchell et al., 2013; Möller et al., 2013; Sowers, 2006, 2010; WAIS Divide Project Members, 2015), see Table S1. These could be modified to account for representational uncertainty associated with the use of a coarse box model, but we have not done this here.

Uncertainty surrounding the isotopic signatures or fractionation factors for sources and sinks are taken into account by sampling from prior distributions. The mean values are detailed in supporting information Table S2 for sources (Etiope et al., 2008; Fisher et al., 2017; Miller, 2005; Sherwood et al., 2017; Snover et al., 2000; Thornton et al., 2016; Whiticar & Schaefer, 2007) and sinks (DeMore, 1993; Gierczak et al., 1997; Saueressig et al., 2001). The uncertainty estimates are given in Table S3 for sources (Etiope et al., 2008; Fischer et al., 2008; Quay et al., 1999; Sherwood et al., 2016; Snover et al., 2000) and sinks (Röckmann et al., 2011; Saueressig et al., 1995, 1996, 2001; Snover & Quay, 2000).

The prior information (summarized in Table 1) on the five methane source terms are normal distributions, with mean values equal to the LGM simulated values from H17, except for hydrate and geological sources for which the preindustrial values are used. The standard deviation of these prior distributions is set to the average of top-down estimates of Kirschke et al. (2013). Assuming the quoted ranges are representative of the 95% limits, these equal 13%. We double this value to account for additional uncertainty for past time periods. Since modern biomass burning rates are influenced by anthropogenic activity (Bowman et al., 2009), we take a range from the literature of 14.3 $TgCH_4$/year (Lamarque et al., 2010) and 37 $TgCH_4$/year (Thonicke et al., 2005) and derive a normal distribution standard deviation of approximately 4 $TgCH_4$/year. The geological and hydrates terms are also subject to wider uncertainties (Etiope et al., 2008; Petrenko et al., 2017. We assume that these terms have a similar relative uncertainty as biomass burning, that is, a standard deviation of 2.8 $TgCH_4$/year.

Any change in biomass burning CH_4 would be accompanied by a change in wildfire emission of nitrogen oxides and carbon monoxide which would impact on the CH_4 lifetime. In H17 varying the LGM fire source between 10% and 84% of the late preindustrial source total, led to 2% and 8% relative increase in CH_4 lifetime. Thus, we include this co-variation.

The MCMC algorithm was run for one million iterations, with the initial 250,000 iterations discarded (Gilks et al., 1995). The four cases in Figure 3 are using (i) only CH_4 concentration observations (green), (ii) both the concentration and $\delta^{13}CH_4$ or (iii) δDCH_4, and (iv) the concentration and both isotopes (blue). The top three panels show the fit to the LGM ice core observations in each case. In the lower panels, the distributions of the model parameters are shown (i.e., inferred source strengths at the LGM). Prior distributions are shown by dashed lines.

The results show that the MCMC algorithm reproduces the observed LGM methane concentration, $\delta^{13}CH_4$ and $\delta D(CH_4)$ well. All four cases point to a reduced tropical wetland CH_4 flux at the LGM. The posterior mean derived by considering all observations is 32.0 $\pm$ 5.0 $TgCH_4$/year (mean $\pm$1 standard deviation), and this is 59% of the prior mean (54.7 $\pm$ 15 $TgCH_4$/year), or 44% of the preindustrial value. Northern wetlands are inferred to decrease to 22% of the preindustrial value when all observations are included, a reduction of 33% relative to the prior distribution. The prior and posterior are less divergent for termite, geological, and hydrate source strengths. The geological term is the only source with an increase at the LGM (posterior mean is 10.5 $\pm$ 2.5 $TgCH_4$/yr), prior (10.0 $\pm$ 2.8 $TgCH_4$/year). This emerges in both the all data and the concentration with $\delta^{13}C$ cases. It is driven by the high $\delta^{13}CH_4$ of geological sources (−33‰) and the model-informed prior distribution (H17) on biomass burning (the other $\delta^{13}CH_4$-enriched source), which points to a reduction in biomass burning at the LGM.

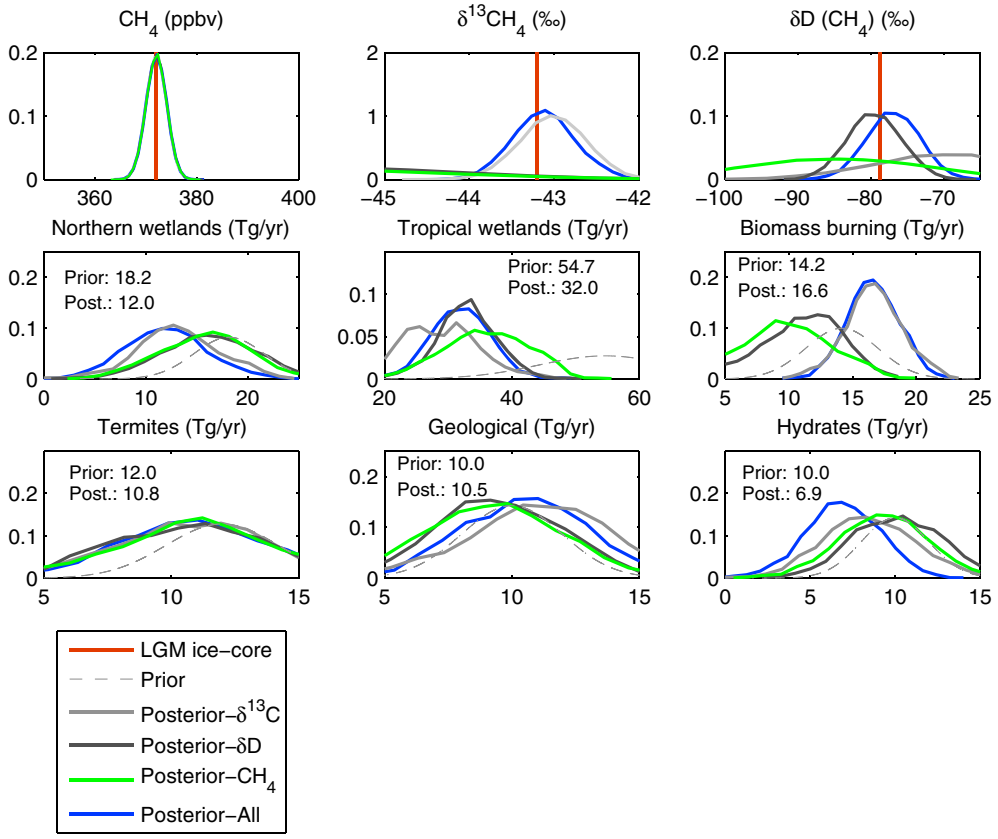

Figure 3. Posterior probability density functions of Last Glacial Maximum CH_4 concentrations (ppbv), isotopes (‰), and emission rates ($TgCH_4$/year) as inferred with the MCMC algorithm, with annotated prior and posterior mean values (for the all case as shown by blue curves). The four different posteriors show the impact of including all of the observations, the CH_4 concentration alone or combined with the $\delta^{13}CH_4$ or the δDCH_4. The strongest overall constraint comes from the concentration itself, while the deuterium appears to have the weakest overall influence. The influence of $\delta^{13}CH_4$ mostly manifests as a subtle increase in the mean for both geological and biomass burning fluxes (compare light gray versus green curves). The posterior mean for the geological emissions is the only term for which the inferred Last Glacial Maximum value is close to or higher than the preindustrial value.

In the remaining cases, the solutions that stem from only considering the CH_4 concentration alone or with one isotope type, are caused by the interplay between satisfying the prior information and the observations. For example, in the CH_4-only case, both the biomass burning and geological terms are reduced, because the isotopic constraint is absent and because this allows the wetland source to stay nearer to its prior distribution.

The inferences drawn separately from the $\delta^{13}CH_4$ and $\delta D(CH_4)$ are not entirely consistent. Including the concentration with deuterium leads to an increased hydrate flux and a reduced biomass burning term, while $\delta^{13}CH_4$ leads to the opposite behavior. Overall the reduced tropical wetlands are required to satisfy the concentration constraint, while relatively high biomass burning and geological sources are required by the $\delta^{13}CH_4$. The main constraint from δD is more difficult to isolate. It acts in a compensatory manner between the biomass burning and hydrate terms.

Doubling the observational or prior uncertainty estimates has very little impact on the posterior distributions (Figures S2 and S3). With uniform priors (Figure S4), the posterior distributions show even stronger reductions in both extratropical and tropical wetlands (for example, the posterior mean for tropical wetlands is 61% lower than the prior mean). The termite term is significantly higher than assumed with the original prior, but this is inconsistent with the best estimate for the LGM emission strength (H17). This demonstrates the potential value of introducing prior information. We also tested the approach by using the prior for the LGM but with the CH_4 concentration and isotope observations replaced with the late preindustrial values (see Figure S5). Overall, the sensitivity tests compared in Figures S2–S5, support the main conclusions above.

5. Discussion

Using recent process-based Earth Model simulations of the late preindustrial and LGM methane budget, we calculate the likely impact on atmospheric CH_4 isotopes. This shows that current estimates of the methane cycle underestimate both the concentration change and the isotopic response, even accounting for uncertainty in LGM biomass burning emissions.

We extend previous work (Kaplan, 2002; Ringeval et al., 2013; H17) to calculate the potential influence of leaf $\delta^{13}C$ of terrestrial vegetation on the natural sources of CH_4 (i.e., wetlands and biomass burning). Though the results are likely model dependent (because they are sensitive to the spatial distribution of emissions), they suggest a limited role for changes in the isotopic discrimination of vegetation in the glacial-interglacial changes in $\delta^{13}CH_4$. This raises the question of why there is such a clear correlation between $\delta^{13}CH_4$ and CO_2 in the ice core record, which Möller et al. (2013) have attributed in part to the influence of leaf ^{13}C on the emissions of CH_4 from tropical wetlands.

We also found that climatically driven changes in the boundary layer Cl sink contributed only 0.12‰ to the $\delta^{13}CH_4$ at the LGM relative to the preindustrial, consistent with past work (Levine, Wolff, Jones, & Sime, 2011). A substantial increase in sea salt aerosols at high latitudes during the LGM (Fischer et al., 2007) may have enhanced the Cl sink (Levine, Wolff, Jones, & Sime, 2011), but this is yet to be included in models (Levine et al., 2014). We have also not included any terrestrial sources of CH_3Cl.

We used a probabilistic approach to show that both biomass burning and geologic sources of methane may have played a role in setting the observed enrichment of atmospheric CH_4 (Bock et al., 2017). The latter is supported by the proposed sea level control on marine seepage of CH_4 (Etiope et al., 2008; Luyendyk et al., 2005). Hence, our modeling results are potentially consistent with the Möller et al. (2013) observations because of the high degree of covariance between CO_2, sea level, and other climatically relevant variables on a glacial-interglacial timescale.

Further, the estimated modern day natural geological CH_4 source of around 54 $TgCH_4$/year (Kirschke et al., 2013) cannot be reconciled with the required reduction in total methane sources at the LGM (H17). This is because the geological source likely increased at the LGM and because 54 $TgCH_4$/year is a substantial fraction of the natural source. Recent mass balance calculations based on late glacial $^{14}CH_4$ measurements (Petrenko et al., 2017) also support this.

The inferred large reduction in wetland emissions is not simulated by H17 and is at the extreme limit of the uncertainty range of recent model-based estimates of the LGM-PI wetland change, (29% to 67%: Hopcroft et al., 2014; Ringeval et al., 2013; Weber et al., 2010). However, several processes (e.g., wetland carbon cycle processes, nutrient status, and tree-mediated transport) that are not properly represented (Melton et al., 2013; Pangala et al., 2017; Wania et al., 2013; H17) need to be evaluated.

6. Conclusions

Current process-based estimates suggest that a 50% reduction in sources is required to explain the CH_4 concentration during the LGM. Bottom-up estimates of emissions fail to replicate this. A comprehensive Earth System model study (H17) also underestimates the changes in CH_4 stable isotopes. Accounting for changes in isotopic discrimination of vegetation does not explain the observed LGM-PI $\delta^{13}CH_4$ shift.

We applied a Bayesian framework to resolve the potentially conflicting information from models and observations. The results suggest that the concentration change was predominantly driven by wetlands, but the inferred emissions response is at the extreme end of model predictions. The isotopic change is either driven by a relatively limited reduction in biomass burning at the LGM, perhaps brought about by human activities (Kaplan et al., 2016), or an increase in nonhydrate geological CH_4 emissions. Future work needs to better understand the climatic sensitivity of natural CH_4 sources, including wetland and geological terms, and this study suggests that incorporation of CH_4 stable isotopes into Earth System model simulations is one avenue for further progress.

Acknowledgments
P. O. H. was funded by the NERC projects NE/I010912/1 and NE/P002536/1, by a Past Earth Network Feasibility Study (EP/M008363/1), and presently by a University of Birmingham Fellowship. J. O. K. was supported by the European Research Council (313797, COEVOLVE). HadGEM2-ES simulations were performed using UK national computing facility ARCHER (http://www.archer.ac.uk). We thank CMS at NCAS for maintaining HadGEM2-ES on this facility. HadGEM2-ES output is available for further analysis from http://www.bridge.bris.ac.uk/resources/simulations.

References

Allan, W., Struthers, H., & Lowe, D. (2007). Methane carbon isotope effects caused by atomic chlorine in the marine boundary layer: Global model results compared with Southern Hemisphere measurements. *Journal of Geophysical Research*, *112*, D04306. https://doi.org/10.1029/2006JD007369

Blair, N., Boehme, S., & Carter, W., Jr. (1993). The carbon isotope biogeochemistry of methane production in anoxic sediments: 1. Field observations. In R. S. Oremland (Ed.), *Biogeochemistry of Global Change* (pp. 574–593). New York: Chapman and Hall.

Bock, M., Schmitt, J., Beck, J., Seth, B., Chappellaz, J., & Fischer, H. (2017). Glacial/interglacial wetland, biomass burning, and geologic methane emissions constrained by dual stable isotopic CH_4 ice core records. *Proceedings of the National Academy of Sciences of the United States of America*, *114*, E5778–E5786. https://doi.org/10.1073/pnas.1613883114

Booth, B., Dunstone, N., Halloran, P., Andrews, T., & Bellouin, N. (2012). Aerosols implicated as a prime driver of twentieth-century North Atlantic climate variability. *Nature*, *484*(7393), 228–232. https://doi.org/10.1038/nature10946

Bousquet, P., Ringeval, B., Pison, I., Dlugokencky, E., Brunke, E.-G., Carouge, C., et al. (2011). Source attribution of the changes in atmospheric methane for 2006–2008. *Atmospheric Chemistry and Physics*, *11*, 3689–3700.

Bowman, D., Balch, J., Artaxo, P., Bond, W., Carlson, J. M., Cochrane, M. A., et al. (2009). Fire in the Earth System. *Science*, *324*, 481–484.

Bragg, F., Prentice, I., Harrison, S., Eglinton, G., & Foster, P. (2013). Stable isotope and modelling evidence for CO_2 as a driver of glacial–interglacial vegetation shifts in southern Africa. *Biogeosciences*, *10*, 2001–2010. https://doi.org/10.5194/bg-10-2001-2013

Caesar, J., Palin, E., Liddicoat, S., Lowe, J., Burke, E., Pardaens, A., et al. (2013). Response of the HadGEM2 Earth System model to future greenhouse gas emissions pathways to the year 2300. *Journal of Climate*, *26*, 3275–3284.

Chanton, J., Rutkowski, C., Schwartz, C., Ward, D., & Boring, L. (2000). Factors influencing the stable carbon isotopic signature of methane from combustion and biomass burning. *Journal of Geophysical Research*, *105*(D2), 1867–1877.

Collins, W., Bellouin, N., Doutriaux-Boucher, M., Gedney, N., Halloran, P., Hinton, T., et al. (2011). Development and evaluation of an Earth-system model—HadGEM2. *Geoscientific Model Development*, *4*, 1051–1075. https://doi.org/10.5194/gmd-4-1051-2011

Conrad, R. (2005). Quantification of methanogenic pathways using stable carbon isotopic signatures: A review and a proposal. *Organic Geochemistry*, *36*, 739–752.

Cox, P. (2001). Description of the TRIFFID dynamic global vegetation model, Hadley Centre, Met Office, Technical Note 24, UK.

DeMore, W. (1993). Rate constant ratio for the reaction of OH with CH3D and CH4. *Journal of Physical Chemistry*, *97*, 8564–8566.

Denison, D., Holmes, C., Mallick, B., & Smith, A. (2002). *Bayesian methods for nonlinear classification and regression*. Chichester: John Wiley.

Etiope, G., Milkov, A., & Derbyshire, E. (2008). Did geologic emissions of methane play any role in Quaternary climate change? *Global and Planetary Change*, *61*, 79–88.

Ferretti, D., Miller, J., White, J., Etheridge, D., Lassey, K., Lowe, D., et al. (2005). Unexpected changes to the global methane budget over the past 2000 years. *Science*, *309*, 1714–1717.

Fischer, H., Siggaard-Andersen, M.-L., Ruth, U., Röthlisberger, R., & Wolff, E. (2007). Glacial/interglacial changes in mineral dust and sea-salt records in polar ice cores: Sources, transport, and deposition. *Reviews of Geophysics*, *45*, RG1002. https://doi.org/10.1029/2005RG000192

Fischer, H., Behrens, M., Bock, M., Richter, U., Schmitt, J., Loulergue, L., et al. (2008). Changing boreal methane sources and constant biomass burning during the last termination. *Nature*, *452*, 864–867. https://doi.org/10.1038/nature06825

Fisher, R., France, J., Lowry, D., Lanoisellé, M., Brownlow, R., Pyle, J., et al. (2017). Measurement of the ^{13}C isotopic signature of methane emissions from Northern European wetlands. *Global Biogeochemical Cycles*, *31*, 605–623. https://doi.org/10.1002/2016GB005504

Gedney, N., Cox, P., & Huntingford, C. (2004). Climate feedback from wetland methane emissions. *Geophysical Research Letters*, *31*, L20503. https://doi.org/10.1029/2004GL020919

Gierczak, T., Talukdar, R., Herdndon, S., Vaghjiani, G. L., & Ravishankara, A. R. (1997). Rate coefficients for the reactions of hydroxyl radicals with methane and deuterated methanes. *Journal of Physical Chemistry*, *101*, 3125–2134.

Gilks, W., Richardson, S., & Spiegelhalter, D. (1995). Introducing Markov chain Monte Carlo methods. In W. R. Gilks, S. Richardson, & D. J. Spiegelhalter (Eds.), *Markov chain Monte Carlo in practice*. London: Chapman and Hall.

HadGEM2 Development Team (2011). The HadGEM2 family of Met Office unified model climate configurations. *Geoscientific Model Development*, *4*, 7233–757. https://doi.org/10.5194/gmd-4-723-2011

Harper, A., Cox, P., Friedlingstein, P., Wiltshire, A., Jones, C., Sitch, S., et al. (2016). Improved representation of plant functional types and physiology in the Joint UK Land Environment Simulator (JULES v4.2) using plant trait information. *Geoscientific Model Development*, *9*, 2415–2440. https://doi.org/10.5194/gmd-9-2415-2016

Hayman, G., O'Connor, F., Dalvi, M., Clark, D., Gedney, N., Huntingford, C., et al. (2014). Comparison of the HadGEM2 climate-chemistry model against in situ and SCIAMACHY atmospheric methane data. *Atmospheric Chemistry and Physics*, *14*, 13,257–13,280.

Hopcroft, P., & Valdes, P. (2015). Last Glacial Maximum constraints on the Earth System model HadGEM2-ES. *Climate Dynamics*, *45*(5), 1657–1672. https://doi.org/10.1007/s00382-014-2421-0

Hopcroft, P., Valdes, P., Wania, R., & Beerling, D. (2014). Limited response of peatland CH_4 emissions to abrupt changes in Atlantic ocean circulation in glacial states. *Climate of the Past*, *10*, 137–154. https://doi.org/10.5194/cp-10-137-2014

Hopcroft, P., Valdes, P., O'Connor, F., Kaplan, J., & Beerling, D. (2017). Understanding the glacial methane cycle. *Nature Communications*, *8*, 14383. https://doi.org/10.1038/ncomms14383

Jones, C., Hughes, J., Bellouin, N., Hardiman, S., Jones, G., Knight, J., et al. (2011). The HadGEM2-ES implementation of CMIP5 centennial simulations. *Geoscientific Model Development*, *4*, 543–570.

Kandlbauer, J., Hopcroft, P., Valdes, P., & Sparks, R. (2013). Climate and carbon cycle response to the 1815 Tambora volcanic eruption. *Journal of Geophysical Research: Atmospheres*, *118*, 12,497–12,507. https://doi.org/10.1002/2013JG019767

Kaplan, J. (2002). Wetlands at the Last Glacial Maximum: Distribution and methane emissions. *Geophysical Research Letters*, *29*(6), 1079. https://doi.org/10.1029/2001GL013366

Kaplan, J., Prentice, I., & Buchmann, N. (2002). The stable carbon isotope composition of the terrestrial biosphere: Modeling at scales from the leaf to the globe. *Global Biogeochemical Cycles*, *16*(4), 1060. https://doi.org/10.1029/2001GB001403

Kaplan, J., Prentice, I., Knorr, W., & Valdes, P. (2002). Modeling the dynamics of terrestrial carbon storage since the Last Glacial Maximum. *Geophysical Research Letters*, *29*(22), 2074. https://doi.org/10.1029/2002GL015230

Kaplan, J., Folberth, G., & Hauglustaine, D. (2006). Role of methane and biogenic volatile organic compound sources in the late glacial and Holocene fluctuations of atmospheric methane concentrations. *Global Biogeochemical Cycles*, *20*, GB2016. https://doi.org/10.1029/2005GB002590

Kaplan, J., Bigelow, N. H., Prentice, I. C., Harrison, S. P., Bartlein, P. J., Christensen, T. R., et al. (2003). Climate change and Arctic ecosystems: 2. Modeling, paleodata-model comparisons, and future projections. *Journal of Geophysical Research*, *108*(D19), 8171. https://doi.org/10.1029/2002JD002559

Kaplan, J., Pfeiffer, M., Kolen, J., & Davis, B. (2016). Large scale anthropogenic reduction of forest cover in Last Glacial Maximum Europe. *PLoS One*, *11*(11), e0166726. https://doi.org/10.1371/journal.pone.0166726

Kirschke, S., Bousquet, P., Ciais, P., Saunois, M., Canadell, J. G., Dlugokencky, E. J., et al. (2013). Three decades of global methane sources and sinks. *Nature Geoscience*, *6*, 813–822. https://doi.org/10.1038/NGEO1955

Lamarque, J.-F., Bond, T. C., Eyring, V., Heil, A., Klimont, Z., Lee, D., et al. (2010). Historical (1850–2000) gridded anthropogenic and biomass burning emissions of reactive gases and aerosols: Methodology and application. *Atmospheric Chemistry and Physics*, *10*, 7017–7039.
Lassey, K., Lowe, D., & Manning, M. (2000). The trend in atmospheric methane $\delta^{13}C$ and implications for isotopic constraints on the global methane budget. *Global Biogeochemical Cycles*, *14*(1), 41–49.
Levine, J., Wolff, E., Jones, A., Sime, L., Valdes, P., Archibald, A., et al. (2011). Reconciling the changes in atmospheric methane sources and sinks between the Last Glacial Maximum and the pre-industrial era. *Geophysical Research Letters*, *38*, L23804. https://doi.org/10.1029/2011GL049545
Levine, J., Wolff, E., Jones, A., & Sime, L. (2011). The role of atomic chlorine in glacial-interglacial changes in the carbon-13 content of atmospheric methane. *Geophysical Research Letters*, *38*, L04801. https://doi.org/10.1029/2010GL046122
Levine, J., Yang, X., Jones, A. E., & Wolff, E. W. (2014). Sea salt as an ice core proxy for past sea ice extent: A process-based model study. *Journal of Geophysical Research: Atmospheres*, *119*, 5737–5756. https://doi.org/10.1002/2013JD020925
Lloyd, J., & Farquhar, G. (1994). ^{13}C discrimination during CO_2 assimilation by the terrestrial biosphere. *Oecologia*, *99*, 201–215.
Loulergue, L., Schilt, A., Spahni, R., Masson-Delmotte, V., Blunier, T., Lemieux, B., et al. (2008). Orbital and millennial-scale features of atmospheric CH_4 over the past 800,000 years. *Nature*, *453*, 383–386.
Luyendyk, B., Kennett, J., & Clark, J. (2005). Hypothesis for increased atmospheric methane input from hydrocarbon seeps on exposed continental shelves during glacial low sea level. *Marine and Petroleum Geology*, *22*, 591–596.
Marthews, T., Dadson, S., Lehner, B., Abele, S., & Gedney, N. (2015). A high-resolution global dataset of topographic index values for use in large-scale hydrological modelling. *Hydrology and Earth System Sciences*, *19*, 91–104.
Melton, J., Wania, R., Hodson, E., Poulter, B., Ringeval, B., Spahni, R., et al. (2013). Present state of global wetland and wetland CH_4 modelling: Conclusions from a model intercomparison project (WETCHIMP). *Biogeosciences*, *10*, 753–788. https://doi.org/10.5194/bg-10-753-2013
Miller, J. (2005). chap The carbon isotopic composition of atmospheric methane and its constraint on the global methane budget. In L. Flanagan, J. Ehleringer, & D. Pataki (Eds.), *Stable isotopes and biosphere-atmosphere interactions: Processes and Biological Controls* (Vol. 16, pp. 288–312). San Diego, CA: Elsevier Academic Press.
Mitchell, L., Brook, E., Lee, J. E., Buizert, C., & Sowers, T. (2013). Constraints on the Late Holocene Anthropogenic Contribution to the Atmospheric Methane Budget. *Science*, *342*, 964–966.
Möller, L., Sowers, T., Bock, M., Spahni, R., Behrens, M., Schmitt, J., et al. (2013). Independent variations of CH4 emissions and isotopic composition over the past 160,000 years. *Nature Geoscience*, *6*, 885–891. https://doi.org/10.1038/NGEO1922
Moosavi, S., & Crill, P. (1998). CH4 oxidation by tundra wetlands as measured by a selective inhibitor technique. *Journal of Geophysical Research*, *103*(D22), 29,093–29,106.
Murray, L., Mickley, L. J., Kaplan, J. O., Sofen, E. D., Pfeiffer, M., Alexander, B., et al. (2014). Factors controlling variability in the oxidative capacity of the troposphere since the Last Glacial Maximum. *Atmospheric Chemistry and Physics*, *14*, 3589–3622. https://doi.org/10.5194/acp-14-3589-2014
Myhre, G., Shindell, D., Breon, F.-M., Collins, W., Fuglestvedt, J., Huang, J., et al. (2013). Anthropogenic and natural radiative forcing. In T. Stocker, et al. (Eds.), *Climate Change 2013: The physical science basis. Contribution of Working Group I to the Fifth Assessment Report of the Intergovernmental Panel on Climate Change*. Cambridge, UK and New York: Cambridge University Press.
Nisbet, E., Dlugokencky, E. J., Manning, M. R., Lowry, D., Fisher, R. E., France, J. L., et al. (2016). Rising atmospheric methane: 2007–2014 growth and isotopic shift. *Global Biogeochemical Cycles*, *30*, 1356–1370. https://doi.org/10.1002/2016GB005406
O'Connor, F., Johnson, C., Morgenstern, O., Abraham, N., Braesicke, P., Dalvi, M., et al. (2014). Evaluation of the new UKCA climate-composition model—Part 2: The troposphere. *Geoscientific Model Development*, *7*, 41–91. https://doi.org/10.5194/gmd-7-41-2014
Pangala, S., Enrich-Prast, A., Basso, L., Peixoto, R. B., Bastviken, D., Hornibrook, E. R. C., et al. (2017). Large emissions from floodplain trees close the Amazon methane budget. *Nature*, *552*, 230–234. https://doi.org/10.1038/nature24639
Petrenko, V., Smith, A., Schaefer, H., Riedel, K., Brook, E., Baggenstos, D., et al. (2017). Minimal geological methane emissions during the Younger Dryas-Preboreal abrupt warming event. *Nature*, *548*, 443–446. https://doi.org/10.1038/nature23316
Pfeiffer, M., Spessa, A., & Kaplan, J. (2013). A model for global biomass burning in preindustrial time: LPJ-LMfire (v1.0). *Geoscientific Model Development*, *6*, 643–685. https://doi.org/10.5194/gmd-6-643-2013
Platt, U., Allan, W., & Lowe, D. (2004). Hemispheric average Cl atom concentration from $^{13}C/^{12}C$ ratios in atmospheric methane. *Atmospheric Chemistry and Physics*, *4*, 2393–2399.
Prather, M., Holmes, C., & Hsu, J. (2012). Reactive greenhouse gas scenarios: Systematic exploration of uncertainties and the role of atmospheric chemistry. *Geophysical Research Letters*, *39*, L09803. https://doi.org/10.1029/2012GL051440
Quay, P., Statesman, J., Wilbur, D., Snover, A., Dlugokencky, E., & Brown, T. (1999). The isotopic composition of atmospheric methane. *Global Biogeochemical Cycles*, *13*(2), 445–461.
Rigby, M., Montzka, S., Prinn, R., White, J. W. C., Young, D., OŠDoherty, S., et al. (2017). Role of atmospheric oxidation in recent methane growth. *Proceedings of the National Academy of Sciences of the United States of America*, *114*(21), 5373–5377.
Ringeval, B., Hopcroft, P., Valdes, P., Ciais, P., Ramstein, G., Dolman, A., & Kageyama, M. (2013). Response of methane emissions from wetlands to the Last Glacial Maximum and an idealised Dansgaard-Oeschger event: Insights from two models of different complexity. *Climate of the Past*, *9*, 149–171. https://doi.org/10.5194/cp-0-149-2013
Röckmann, T., Brass, M., Borchers, R., & Engel, A. (2011). The isotopic composition of methane in the stratosphere: high-altitude balloon sample measurements. *Atmospheric Chemistry and Physics*, *11*, 13,287–13,304. https://doi.org/10.5194/acp-11-13287-2011
Sanderson, M. (1996). Biomass of termites and their emission of methane and carbon dioxide: A global database. *Global Biogeochemical Cycles*, *10*(4), 543–557.
Saueressig, G., Bergamaschi, P., Crowley, J., Fischer, H., & Harris, G. (1995). Carbon kinetic isotope effect in the reaction CH_4 with Cl atoms. *Geophysical Research Letters*, *22*(10), 1225–1228.
Saueressig, G., Bergamaschi, P., Crowley, J., Fischer, H., & Harris, G. (1996). D/H kinetic isotope effect in the reaction CH_4 + Cl. *Geophysical Research Letters*, *23*(24), 3619–3622.
Saueressig, G., Bergamaschi, P., Crowley, J., Fischer, H., & Harris, G. (2001). Carbon 13 and D kinetic isotope effects in the reactions of CH_4 with $O(^1D)$ and OH: New laboratory measurements and their implications for the isotopic composition of stratospheric methane. *Journal of Geophysical Research*, *D19*, 23,127–23,138.
Schaefer, H., & Whiticar, M. (2008). Potential glacial-interglacial changes in stable carbon isotope ratios of methane sources and sink fractionation. *Global Biogeochemical Cycles*, *22*, GB1001. https://doi.org/10.1029/2006GB002889
Schaefer, H., Mikaloff Fletcher, S., Veidt, C., Lassey, K., Brailsford, G., Bromley, T., et al. (2016). A 21st century shift from fossil-fuel to biogenic methane emissions indicated by $^{13}CH_4$. *Science*, *352*, 80–84. https://doi.org/10.1126/science.aad2705

Scheff, J., Seager, R., Liu, H., & Coats, S. (2017). Are glacials dry? Consequences for paleoclimatology and for greenhouse warming. *Journal of Climate*, *30*, 6593–6609. https://doi.org/10.1175/JCLI-D-16-0854.1

Schmitt, J., Schneider, R., Elsig, E., Leuenberger, D., Lourantou, A., Chappellaz, J., et al. (2012). Carbon isotope constraints on the deglacial CO_2 rise from ice cores. *Science*, *336*, 711–714.

Sherwood, O., Schwietzke, S., Arlin, V., & Etiope, G. (2016). Global inventory of fossil and non-fossil methane $\delta^{13}C$ source signature measurements for improved atmospheric modeling (Tech. Rep.). U.S. National Oceanic and Atmospheric Administration. https://doi.org/10.15138/G37P4D

Sherwood, O., Schwietzke, S., Arling, V., & Etiope, G. (2017). Global inventory of gas geochemistry data from fossil fuel, microbial and burning sources, version 2017. *Earth System Science Data*, *9*, 639–656. https://doi.org/10.5194/essd-9-639-2017

Singarayer, J., & Valdes, P. (2010). High-latitude climate sensitivity to ice-sheet forcing over the last 120 kyr. *Quaternary Science Reviews*, *29*(1–2), 43–55. https://doi.org/10.1016/j.quascirev.2009.10.011

Snover, A., & Quay, P. (2000). Hydrogen and carbon kinetic isotope effects during soil uptake of atmospheric methane. *Global Biogeochemical Cycles*, *14*(1), 25–39.

Snover, A., Quay, P., & Has, W. (2000). The D/H content of methane emitted from biomass burning. *Global Biogeochemical Cycles*, *14*(1), 11–24.

Sowers, T. (2006). Late Quaternary atmospheric CH_4 isotope record suggests marine clathrates are stable. *Science*, *311*, 838–840.

Sowers, T. (2010). Atmospheric methane isotope records covering the Holocene period. *Quaternary Science Reviews*, *29*, 213–221.

Thonicke, K., Prenctice, I., & Hewitt, C. (2005). Modeling glacial-interglacial changes in global fire regimes and trace gas emissions. *Global Biogeochemical Cycles*, *19*, GB3008. https://doi.org/10.1029/2004GB002278

Thornton, B., Wik, M., & Crill, P. (2016). Double-counting challenges the accuracy of high-latitude methane inventories. *Geophysical Research Letters*, *43*, 12,569–12,577. https://doi.org/10.1002/2016GL071772

Tyler, S., Zimmerman, P., Cumberbatch, C., Greenberg, J., Westberg, C., & Darlington, J. (1988). Measurements and interpretation of $\delta^{13}C$ of methane from termites, rice paddies, and wetlands in Kenya. *Global Biogeochemical Cycles*, *2*(4), 341–355.

Tyler, S., Crill, P., & Brailsford, G. (1994). $^{13}C/^{12}C$ fractionation of methane during oxidation in a temperate forested soil. *Geochimica et Cosmochinica Acta*, *58*(6), 1625–1633.

Valdes, P., Beerling, D., & Johnson, C. (2005). The ice age methane budget. *Geophysical Research Letters*, *32*, L02704. https://doi.org/10.1029/2004GL021004

WAIS Divide Project Members (2015). Precise interpolar phasing of abrupt climate change during the last ice age. *Nature*, *520*, 661–665.

Wania, R., Ross, I., & Prentice, I. C. (2010). Implementation and evaluation of a new methane model within a dynamic global vegetation model: LPJ-WHyMe v1.3.1. *Geoscientific Model Development*, *3*, 565–584. https://doi.org/10.5194/gmd-3-565-2010

Wania, R., Melton, J., Hodson, E., Poulter, B., Ringeval, B., Spahni, R., et al. (2013). Present state of global wetland extent and wetland methane modelling: Methodology of a model intercomparison project (WETCHIMP). *Geoscientific Model Development*, *6*, 617–641.

Weber, S., Drury, A., Toonen, W., & van Weele, M. (2010). Wetland methane emissions during the Last Glacial Maximum estimated from PMIP2 simulations: Climate, vegetation, and geographic controls. *Journal of Geophysical Research*, *115*, D06111. https://doi.org/10.1029/2009JD012110

Whiticar, M. (1999). Carbon and hydrogen isotope systematics of bacterial formation and oxidation of methane. *Chemical Geology*, *161*, 291–314.

Whiticar, M., & Schaefer, H. (2007). Constraining past global tropospheric methane budgets with carbon and hydrogen isotope ratios in ice. *Global Biogeochemical Cycles*, *365*, 1793–1828. https://doi.org/10.1098/rsta.2007.2048

Worden, J., Bloom, A., Pandey, S., Jiang, Z., Worden, H. M., Walker, T. W., et al. (2018). Reduced biomass burning emissions reconcile conflicting estimates of the post-2006 atmospheric methane budget. *Nature Communications*, *8*, 2227. https://doi.org/10.1038/s41467-017-02246-0